AI drives the assessment of lung cancer microenvironment composition

Enzo Gallo [a,*], Davide Guardiani [a], Martina Betti [b,c], Brindusa Ana Maria Arteni [d], Simona Di Martino [d], Sara Baldinelli [b], Theodora Daralioti [a], Elisabetta Merenda [e], Andrea Ascione [f], Paolo Visca [a], Edoardo Pescarmona [a], Marialuisa Lavitrano [g], Paola Nisticò [h], Gennaro Ciliberto [i], Matteo Pallocca [j]

[a] Department of Pathology, IRCCS Regina Elena National Cancer Institute, Rome, Italy
[b] Biostatistics, Bioinformatics and Clinical Trial Center, IRCCS Regina Elena National Cancer Institute, Rome, Italy
[c] Department of Computer, Control and Management Engineering, La Sapienza University of Rome, Rome, Italy
[d] UOC Anatomy Pathology, Biobank IRCCS Regina Elena National Cancer Institute, Istituti Fisioterapici, Ospitalieri IFO, Rome, Italy
[e] Department of Radiological, Oncological and Pathological Sciences, Sapienza University of Rome, Policlinico Umberto I, Rome, Italy
[f] Department of Experimental Medicine, Sapienza University of Rome, Policlinico Umberto I, Rome, Italy
[g] School of Medicine and Surgery, University of Milano-Bicocca, 20900 Monza, Italy
[h] Tumor Immunology and Immunotherapy Unit, IRCCS Regina Elena National Cancer Institute, Rome, Italy
[i] Scientific Direction, IRCCS Regina Elena National Cancer Institute, Rome, Italy
[j] Institute of Experimental Endocrinology and Oncology, National Research Council, Naples, Italy

ARTICLE INFO

ABSTRACT

Purpose: The abundance and distribution of tumor-infiltrating lymphocytes (TILs) as well as that of other components of the tumor microenvironment is of particular importance for predicting response to immunotherapy in lung cancer (LC). We describe here a pilot study employing artificial intelligence (AI) in the assessment of TILs and other cell populations, intending to reduce the inter- or intra-observer variability that commonly characterizes this evaluation.
Design: We developed a machine learning-based classifier to detect tumor, immune, and stromal cells on hematoxylin and eosin-stained sections, using the open-source framework *QuPath*. We evaluated the quantity of the aforementioned three cell populations among 37 LC whole slide images regions of interest, comparing the assessments made by five pathologists, both before and after using graphical predictions made by AI, for a total of 1110 quantitative measurements.
Results: Our findings indicate noteworthy variations in score distribution among pathologists and between individual pathologists and AI. The AI-guided pathologist's evaluations resulted in reduction of significant discrepancies across pathologists: three comparisons showed a loss of significance ($p > 0.05$), whereas other four showed a reduction in significance ($p > 0.01$).
Conclusions: We show that employing a machine learning approach in cell population quantification reduces inter- and intra-observer variability, improving reproducibility and facilitating its use in further validation studies.

Introduction

The application of light microscopy for examining hematoxylin and eosin (H&E) tissue slides remains an essential practice in the field of cancer diagnosis. Such a technique requires the pathologist to accurately identify and distinguish the assorted histopathological components within complex images. For instance, LC histopathology is characterized by a complex interplay of tumor cells, immune cells (lymphocytes, plasma cells, macrophages, and granulocytes), fibroblasts, and endothelial cells.[1] Many of said

measures are valuable biomarkers in the clinical field: several studies show how the density of tumor-infiltrating lymphocytes (TILs) correlates with better clinical outcomes[2,3] such as longer disease-free survival (DFS) or improved overall survival (OS) in multiple cancer types.[4] Nonetheless, studies have found substantial inter-reader variability in the assessment of TILs density using H&E slides and this has limited the use of TILs density as a prognostic marker for non-small cell lung cancer (NSCLC).[5]

Moreover, tumor cell percentage within formalin-fixed paraffin-embedded samples is a critical factor in the biomarker's evaluations using

---

* Corresponding author.
E-mail addresses: enzo.gallo@ifo.it (E. Gallo), davide.guardiani.roma@gmail.com (D. Guardiani), martina.betti@ifo.it (M. Betti), anamaria.arteni@ifo.it (B.A.M. Arteni), simona.dimartino@ifo.it (S. Di Martino), sara.baldinelli@ifo.it (S. Baldinelli), daraliotitheodora@yahoo.it (T. Daralioti), elisabetta.merenda@uniroma1.it (E. Merenda), andrea.ascione@uniroma1.it (A. Ascione), paolo.visca@ifo.it (P. Visca), edoardo.pescarmona@ifo.it (E. Pescarmona), marialuisa.lavitrano@unimib.it (M. Lavitrano), paola.nistico@ifo.it (P. Nisticò), gennaro.ciliberto@ifo.it (G. Ciliberto), matteo.pallocca@cnr.it (M. Pallocca).

Next Generation Sequencing (NGS) panels, such as the ability to detect important low-frequency somatic mutations in target cancer therapy.

Finally, it is known that evaluating the presence and quantity of different cell populations is a process that is time-consuming and subjective. Furthermore, it generates considerable inter- and intra-observer variation and is a qualitative or, at best, semi-quantitative approach.[6–8]

However, research in the field of diagnostic imaging is expanding with promising results. Although diagnosis based on examination of the classic histological slide using optical microscopy remains the gold-standard, in recent years, advances in the digitization of histological specimens have led to digital slides or whole slide images (WSIs) production.[9–11] Recently the Food and Drugs Administration (FDA) approved the use of WSIs for primary diagnostic use.[12,13] In a few years, most new pathology slides will be digitized, enabling the development and clinical implementation of various digital pathology-based diagnostic and prognostic biomarkers that are likely to provide decision support to traditional pathology interpretation in the clinical setting.[1] New analytic approaches include the application of machine learning (ML) in image analysis in various fields such as pathology diagnostic[14] and dermatology.[15]

The advancement of sophisticated ML algorithms has the potential to enhance the analysis of pathological images and assist pathologists in their diagnostic duties, particularly in identifying neoplasms, detecting tumor metastases, and carry out accurate quantifications of distinct cell populations, including tumor and inflammatory cells. Multiple articles have suggested ML methodologies to assist pathologists in quantifying tumor cell fractions on digital scans. However, these endeavors predominantly encounter a common constraint: establishing a dependable ground-truth definition.[16,17] In this work, we evaluate whether ML-based tools may improve pathology workflows to enable in-depth, reproducible, and accurate characterization of the tumor microenvironment, all with a limited manual curation effort and an objective evaluation strategy.

Materials and methods

Whole slide dataset

This study used anonymized archived LC cases from the Regina Elena National Cancer Institute Biobank BBIRE. The dataset consists of scannable images from the surgical removal of LC (Table S1). The original diagnostic slides were derived from sections (4–5 μm thickness) cut from formalin-fixed paraffin-embedded whole-slide blocks H&E stained. Thirty-seven H&E slides were scanned at 0.25 μm /pixel (40×) acquisition resolution using an Aperio AT2 (Leica Biosytems Inc.). Default instrument settings were used for scanning parameters; default autofocus was used and the scanner automatically selected the focus points number, but in a few cases, manual focus was applied to optimize sharpness. A single focal plane was used, without Z-stacking. Images were stored in a proprietary format (.SVS) and uploaded to a local WSI management server (eSlideManager, Leica). Slides were scanned in anonymized format; they were retrospective archival material, and the results did not have any impact on the management of the patient. All patients included in the study provided written Broad Research Usage Informed Consent before surgery.

Machine learning

In this study, integrated tools from *QuPath* v.0.4[18] were used for image analysis. The scanned images of each slide were never analyzed in their entirety but rather an expert pathologist selected regions of interest (ROIs). The selection criteria for the ROIs were meticulously defined to ensure comprehensive representation of the tissue architecture and tumor characteristics. ROIs were chosen based on the presence of well-defined tumor regions, ensuring a diverse and representative dataset. Additionally, areas with sufficient cellularity and minimal artifacts were prioritized to facilitate accurate annotation and subsequent algorithm training. The target cell populations in this study include tumor cells, immune cells, and stromal cells such as fibroblast and endothelial cells. TILs were defined as mononuclear immune cells including lymphocytes and plasma cells.[19] To ensure an accurate analysis of cell populations, we calculated the *stain vector* for each image to perform color deconvolution in order to perform a color normalization for each image. (Fig. 1A). This method allows us to separate the staining components[20] and reduces staining variability and ensures more consistent and accurate tissue analysis (Supplementary Information).

To train and evaluate the cell classification model a total of 82 ROIs, which comprised 41 pairs, were utilized for training the classifier (Fig. 1B). The ROIs were manually drawn to construct the training set from 13 LC H&E digital slides. Each pair is characterized by a comparable number of cells and cell classes. One element of each pair was named *Sample*, whereas the other was assigned as *Training*. *Sample* regions provide learning input, whereas *Training* regions guide model parameter optimization for accurate classification. Next, cell detection within these areas was performed with the deep learning nuclei segmentation algorithm *StarDist* v.4.0.[21] The same set of parameters were used for the segmentation of all the other ROIs drawn. Segmented nuclei were manually annotated within the Sample ROIs. The quantity of cells to be annotated in the *Sample* ROIs was not predetermined but rather deduced throughout the annotation process based on the software's ability to characterize cells in the *Training*. As a result of this dynamic annotation process, the annotation of 370 cells resulted adequate to learn enough features for cell type discrimination. Among these, 150 were labeled as tumor cells, 86 as immune cells, and 132 as stromal cells. Thereafter, a random forest classifier model was trained on the *Training* ROIs, defined in the previous step, using the integrated *QuPath* function *Train object classifier*. The whole training process is documented in the Supplementary Information. This methodology strongly reduces the time dedicated to manual annotation process, while also avoiding overfitting.

To test the classifier, 13 different WSIs of LC H&E distinct from those used in the training set were chosen. A total of 43 annotations were drawn and collectively named *Test* ROIs with an average area of 44,459 square micrometers and a total of 19,477 cells were identified (Fig. 1C). Each classification made by the classifier was critically reviewed by an expert pathologist, identifying false positives and negatives, as well as true positives and negatives for each cell type, to calculate accuracy, sensitivity, and F1 score (Table S2).

AI-pathologist comparative analysis

A ROI, a rectangle containing a representative tumor area, was selected on a further 37 digital slides for comparative analysis with pathologist. The ROI area (5.8 mm^2) was the same for all 37 slide images, within the tumor without including significant areas of necrosis or background tissue. First, all 37 ROIs were classified using the trained model. The pathologists were asked to estimate the percentage of tumor, immune, and stromal cells present in each ROI in two rounds. In the first round (*Round I*), pathologists provided estimates without access to AI results. In the second round (*Round II*), they reconsidered their evaluations, incorporating graphical predictions generated by the AI. Additionally, each pathologist provided ratings on the efficacy of AI classification for each image.

Statistical analysis

Percentage assignments by pathologists and AI were analyzed by non-parametric statistical tests (Kruskal–Wallis and Wilcoxon rank-sum test α = 0.05). For the correlation study, Kendall's correlation coefficient was also performed. All the statistical surveys were conducted using R v. 4.2.2. Comprehensive details regarding the calculations can be found in Supplementary Information.

Results

The effect of AI integration on pathologist evaluations

We conducted a comparative analysis of tumor, immune, and stromal cell assessments in 37 ROIs related to lung cancer (LC), involving five pathologists. This assessment was carried out both before and after integrating AI-generated graphical predictions, resulting in a total of 1110
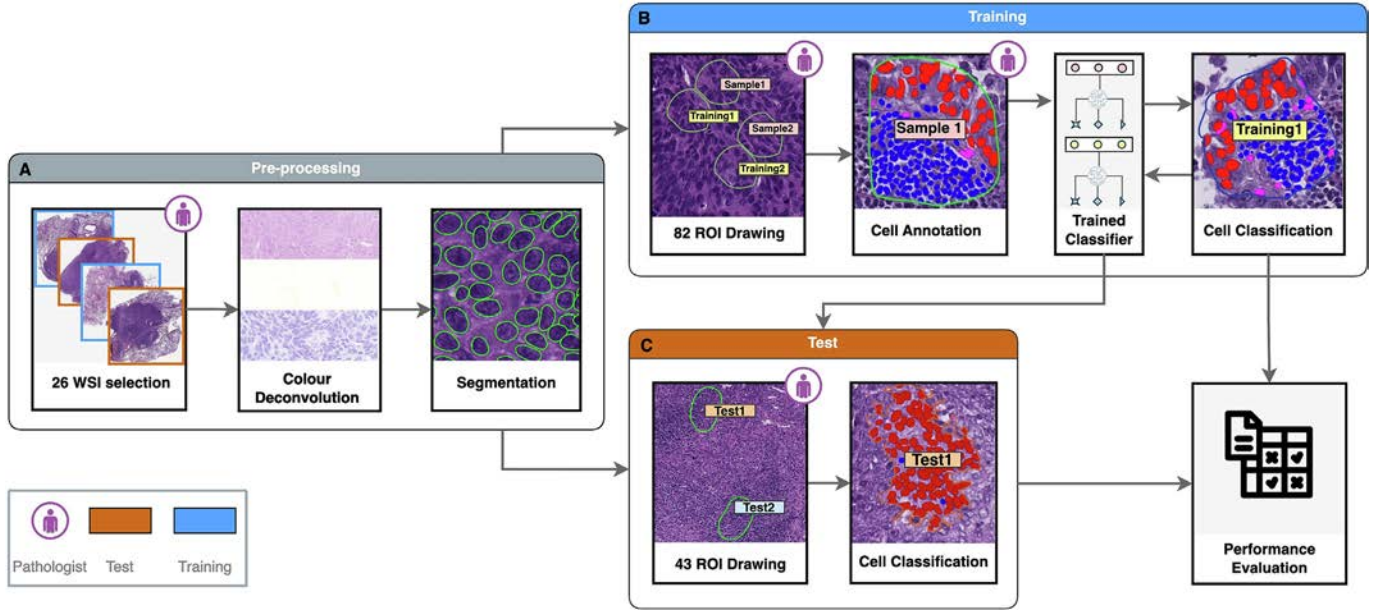
Fig. 1. Graphical Abstract. Depiction of all the steps devoted to the training and the evaluation of the cell classification model. (A) Pre-processing step; (B) training step; (C) test step.

measurements. Overall, in *Round II*, there was a percentual increase in pathologists' assignments of tumor and immune cell classes (49.2% for tumor cells and 32.7% for immune cells in *Round II*, compared to 47.3% for tumor cells and 21.7% for immune cells in *Round I*), whereas there

was a decrease in the percentual assignment of stromal cells (12.1% in *Round II* compared to 21.1% in *Round I*) (Fig. 2A).

Our analysis revealed a significant variation in the pathologists' assignments between the two rounds (p-value < 0.05, Wilcoxon test). Specifically,
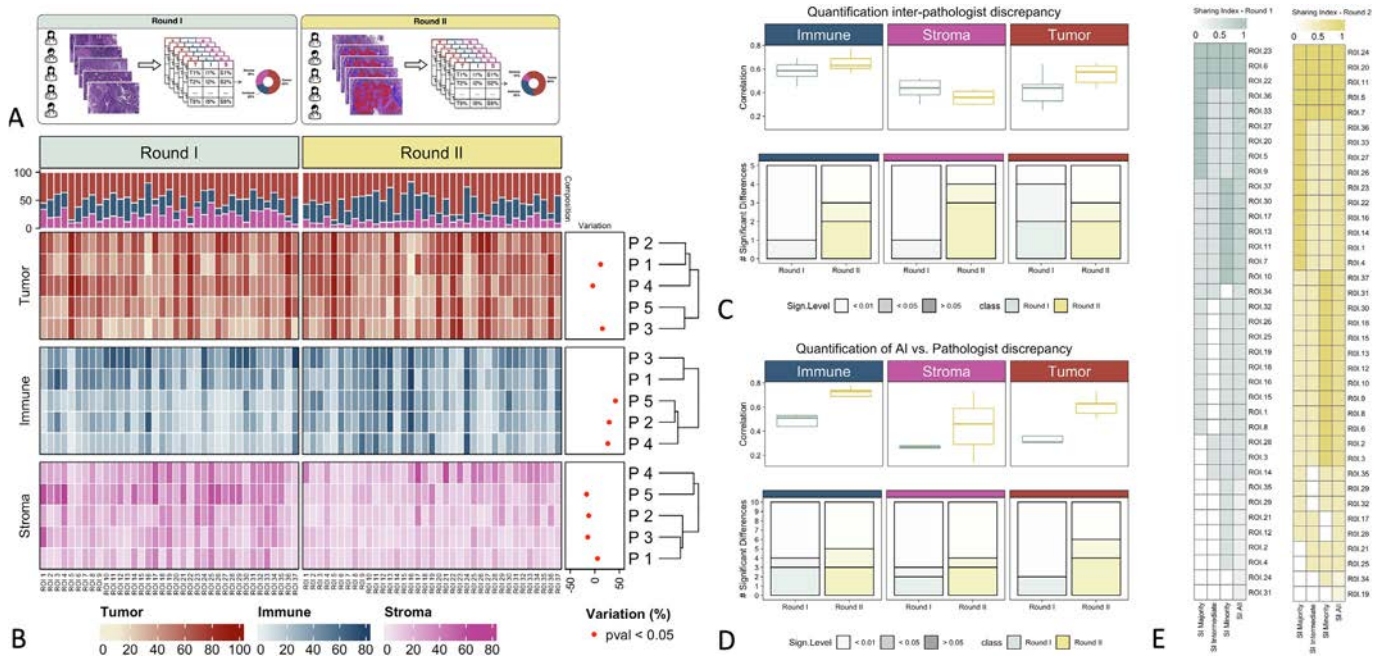
Fig. 2. (A) Illustration of the pathologist's estimation rounds. *Round I* and *Round II* have been performed on the same ROIs with and without the visual support of AI-based cell classification. (B) Pathologist's estimations heatmap. The heatmap shows the percentage of the three cell types assigned by each of the pathologists (P1–P5) for all ROIs. For each ROI, the top annotation describes the average cell composition. Statistically significant percentual variation (across ROIs) in estimates provided by pathologists in *Round I* and *Round II* is described and shown in the right annotation. (C) Quantification of inter-pathologist discrepancy in *Round I* vs *Round II*. The boxplots represent Kendall correlation coefficients, calculated on the estimates given by all couples of pathologists (across ROIs). The bar plots represent the number of significant Wilcoxon tests performed on the estimates given by all couples of pathologists (across ROIs), at two different p-value thresholds (0.05 and 0.01). (D) Quantification of AI vs. Pathologist discrepancy. The boxplots represent Kendall correlation coefficients, calculated on the estimates given by the AI vs. each of the pathologists (across ROIs). The bar plots represent the number of significant Wilcoxon tests performed on the estimates given by the AI vs. each of the pathologists (across ROIs), at two different p-value thresholds (0.05 and 0.01). (E) Sharing Index (SI) heatmap in *Round I* and *Round II* for all three hierarchical positions as well as majority, minority, and intermediate hierarchical position individually. ROIs on the y-axis are sorted from the highest to the lowest global SI. A SI of 1 indicates complete agreement, whereas a SI of 0 indicates the maximum level of discrepancy across pathologists.

a lower level of discrepancy was found across pathologists' assignments in the AI-aided assignments of *Round II*, because three comparisons showed a loss of significance ($p > 0.05$), whereas other four showed a reduction in significance ($p > 0.01$) (Fig. 2B).

Increased pathologist consensus regarding cell estimates

When comparing estimates between pairs of pathologists, there was an overall increase in concordance, as illustrated in Fig. 2C. Specifically, whereas the correlation between estimates for immune and stromal cells remained similar (box plots), the number of significant differences decreased (bar plots). In the case of tumor cells, the number of significant differences (Kruskal–Wallis tests *p*-values <0.05) remained unchanged, yet the correlation increased.

The assessment of pathologists' assignments compared to those generated by AI revealed a notable rise in the average correlation coefficient and a decrease in the number of significant differences across the three cellular populations (Fig. 2D). Taken together, these results indicate that the pathologist's percentage assignments were influenced remarkably by the AI-generated graphical prediction visualization in *Round II*.

AI performance in cell population hierarchy evaluation

Additionally, we aimed to evaluate AI performance based solely on the hierarchy of cell populations determined by pathologists, irrespective of their absolute counts. This approach led to the identification of three categories: majority, intermediate, and minority cell populations. Furthermore, we introduced the concept of a *Sharing Index* to quantify agreement among pathologists regarding hierarchical assignments through an index ranging from 0 to 1 (Supplementary Material).

In *Round I*, all five pathologists assigned the same hierarchy of cell populations in 3 out of 37 ROIs, which increased to 5 in *Round II* (Fig. 2E). The classifier also provided an identical hierarchy in this subset. The Sharing Index generally increased from *Round I* to *Round II*, with half of pathologists agreeing on either the majority or the minority class in 28 ROIs, as opposed to 16 ROIs in *Round I*. The AI assigned the same hierarchy as the majority of pathologists in 22 ROIs, the same hierarchy as the minority (i.e., at least one pathologist) in 6 ROIs, and a different hierarchy from all pathologists in 6 ROIs. These findings indicated an increase in cases of complete agreement and partial agreement among pathologists in *Round II*. Furthermore, in instances of absolute concordance, complete agreement was also observed between pathologists and AI.

Finally, the output of the ML classifier, assessed at the cell level by an expert pathologist, demonstrated high accuracy on the test set (Table S2). AI-assisted classifications received grades from pathologists that were consistently above passing grades, indicating that the classifier effectively categorized the segmented cells in most cases (Table S3).

Discussion

High levels of TILs have emerged as promising prognostic biomarkers in NSCLC patients.[22] Additionally, mounting evidence suggests that TILs are strongly associated with favorable response rates to immunotherapy in NSCLC patients.[23] The International Working Group on Immuno-Oncology has published a set of guidelines for the manual evaluation of cell populations, such as TILs in H&E slides.[24,25] However, despite these standardization efforts, their translational adoption into clinical practice has been limited due to the subjective nature and degree of variability of the assessments.

Assessing cell populations in tissue samples by pathologists can often exhibit significant variability.[26,27] Due to the difficulty of making such assessments, the adjacent microenvironment's cell populations are often overlooked.

In our study, we utilized the *QuPath* software to develop a classifier capable of numerically quantifying tumor, immune, and stromal cells in standard H&E histological sections of LC. Whereas the use of *StarDist* for nuclei

detection and ML-based cell classification appear to be promising tools for cell quantification, potential limitations related to the reliability of the segmentation and classification algorithms must be considered. These limitations may stem from biological artifacts or overfitting of the ML models. To mitigate these limitations and maximize the classifier's capabilities, we took care to avoid artifact-rich areas during the segmentation process and followed a meticulous training procedure.

Our findings reveal that, despite employing the estimate stain vector functions, the classifier exhibited high sensitivity towards the presence of out-of-focus areas and variations in coloration. These variations may be attributed to dissimilar coloring protocols or technical issues, such as suboptimal section thickness and degraded dyes or color variation among different laboratories.[28,29] To overcome this challenge, cutting-edge automatic algorithms have been developed to identify the optimal regions for such analyses, thereby standardizing the quality of whole-slide images utilized in research.[30]

Not only did the ML classifier showed a general high level of accuracy, but played a crucial role in enabling the pathologists to assign more values that are comparable during the second evaluation. As demonstrated there exists a discernible disparity in the assignments of each pathologist even with the AI utilization.

The AI-generated percentage for each cell population is primarily based on the area of segmented nuclei, whereas pathologists consider both the nuclei and the extracellular matrix when evaluating stromal cells. However, the percentages assigned to stroma by the pathologists were reduced (-42.7%) after viewing the AI's graphical predictions, suggesting a potential overestimation of stromal cells by the pathologists in *Round I* due to the challenge associated with detecting individual stromal cells in a complex context, at the expense of the other two cellular components (tumor cells and immune cells), with a percentage increase in Round II of $+4\%$ for tumor cells and $+50.8\%$ for immune cells. This disparity can be attributed to the challenge pathologists encounter in numerically and reproducibly quantifying different cell populations within a given area.[31,32]

In conclusion, our objective was not to create a completely automated ML classifier for cell populations but rather to develop a computer-assisted tool that can aid pathologists in accurately estimating the proportion of various cell populations, resulting in a marked reduction of inter- and intra-observer variability and a significant improvement in reproducibility. Particularly, this tool can be beneficial in scenarios such as determining the percentage of cancer cells for molecular testing or evaluating the degree of immune infiltrate as a prognostic indicator for immunotherapy response.

Author contribution

EG and MP performed study concept and design; EG, MP, DG and MB performed development of methodology and writing, review, and revision of the paper; EG, DG, MB and BAMA, provided acquisition, analysis and interpretation of data, and statistical analysis; DG, MB, SB, BAMA, SDM, TD, EM, AA, PV, EP, MLV, PN, GC, MP provided technical and material support. All authors read and approved the final paper.

Data availability

The datasets generated during and/or analyzed during the current study are available in the github repository DP_BBIRE_ML_CompositionClassifier [https://gitlab.com/bioinfo-ire-release/bbire].

Declaration of competing interest

The authors declare the following financial interests/personal relationships which may be considered as potential competing interests: Matteo Pallocca reports a relationship with Dexma srl that includes: consulting or advisory. If there are other authors, they declare that they have no known competing financial interests or personal relationships that could have appeared to influence the work reported in this article.

Appendix A. Supplementary data

Supplementary data to this article can be found online at https://doi.org/10.1016/j.jpi.2024.100400.

References

1. Corredor G, Wang X, Zhou Y, et al. Spatial architecture and arrangement of tumor-infiltrating lymphocytes for predicting likelihood of recurrence in early-stage non-small cell lung cancer. Clin Cancer Res Off J Am Assoc Cancer Res 2019;25(5). https://doi.org/10.1158/1078-0432.CCR-18-2013.
2. Geng Y, Shao Y, He W, et al. Prognostic role of tumor-infiltrating lymphocytes in lung cancer: a meta-analysis. Cell Physiol Biochem Int J Exp Cell Physiol Biochem Pharmacol 2015;37(4). https://doi.org/10.1159/000438523.
3. Bremnes R, Donnem T, Busund L. Importance of tumor infiltrating lymphocytes in non-small cell lung cancer? Ann Transl Med 2016;4(7). https://doi.org/10.21037/atm.2016.03.28.
4. Bruni D, Angell H, Galon J. The immune contexture and Immunoscore in cancer prognosis and therapeutic efficacy. Nat Rev Cancer 2020;20(11). https://doi.org/10.1038/s41568-020-0285-7.
5. Brambilla E, Le Teuff G, Marguet S, et al. Prognostic effect of tumor lymphocytic infiltration in Resectable non-small-cell lung cancer. J Clin Oncol Off J Am Soc Clin Oncol 2016;34(11). https://doi.org/10.1200/JCO.2015.63.0970.
6. van den Bent M. Interobserver variation of the histopathological diagnosis in clinical trials on glioma: a clinician's perspective. Acta Neuropathol 2010;120(3). https://doi.org/10.1007/s00401-010-0725-7.
7. Elmore J, Longton G, Carney P, et al. Diagnostic concordance among pathologists interpreting breast biopsy specimens. JAMA 2015;313(11). https://doi.org/10.1001/jama.2015.1405.
8. Linder N, Taylor JC, Colling R, et al. Deep learning for detecting tumour-infiltrating lymphocytes in testicular germ cell tumours. J Clin Pathol 2019;72(2):157–164. https://doi.org/10.1136/jclinpath-2018-205328.
9. Farris AB, Cohen C, Rogers TE, Smith GH, From the Department of Pathology EU, Atlanta, Georgia. Whole slide imaging for analytical anatomic pathology and telepathology: practical applications today, promises, and perils. Arch Pathol Lab Med 2023;141(4):542–550. https://doi.org/10.5858/arpa.2016-0265-SA.
10. Evans AJ, Salama ME, Henricks WH, Pantanowitz L. Implementation of whole slide imaging for clinical purposes: issues to consider from the perspective of early adopters. Arch Pathol Lab Med 2017;141(7). https://doi.org/10.5858/arpa.2016-0074-OA.
11. Fraggetta F, Garozzo S, Zannoni G, Pantanowitz L, Rossi E. Routine digital pathology workflow: the Catania experience. J Pathol Inform 2017;8. https://doi.org/10.4103/jpi.jpi_58_17.
12. Evans A, Bauer T, Bui M, et al. US Food and Drug Administration approval of whole slide imaging for primary diagnosis: akey milestone is reached and new questions are raised. Arch Pathol Lab Med 2018;142(11). https://doi.org/10.5858/arpa.2017-0496-CP.
13. Patel A, Balis U, Cheng J, et al. Contemporary whole slide imaging devices and their applications within the modern pathology department: aselected hardware review. J Pathol Inform 2021;12. https://doi.org/10.4103/jpi.jpi_66_21.
14. Araújo T, Aresta G, Castro E, et al. Classification of breast cancer histology images using convolutional neural networks. PLoS One 2017;12(6). https://doi.org/10.1371/journal.pone.0177544.
15. Esteva A, Kuprel B, Novoa RA, et al. Dermatologist-level classification of skin cancer with deep neural networks. Nature 2017;542(7639):115–118. https://doi.org/10.1038/nature21056.
16. Frei A, Oberson R, Baumann E, et al. Pathologist computer-aided diagnostic scoring of tumor cell fraction: a Swiss national study. Mod Pathol Off J US Can Acad Pathol, Inc 2023;36(12). https://doi.org/10.1016/j.modpat.2023.100335.
17. Willis J, Anders R, Torigoe T, et al. Multi-institutional evaluation of pathologists' assessment compared to immunoscore. Cancers 2023;15(16). https://doi.org/10.3390/cancers15164045.
18. Bankhead P, Loughrey M, Fernández J, et al. QuPath: open source software for digital pathology image analysis. Sci Rep 2017;7(1). https://doi.org/10.1038/s41598-017-17204-5.
19. Rakaee M, Adib E, Ricciuti B, et al. Association of machine learning-based assessment of tumor-infiltrating lymphocytes on standard histologic images with outcomes of immunotherapy in patients with NSCLC. JAMA Oncol 2023;9(1). https://doi.org/10.1001/jamaoncol.2022.4933.
20. Ruifrok A, Katz R, Johnston D. Comparison of quantification of histochemical staining by hue-saturation-intensity (HSI) transformation and color-deconvolution. Appl Immunohistochem Mol Morphol AIMM 2003;11(1). https://doi.org/10.1097/00129039-200303000-00014.
21. Schmidt U, Weigert M, Broaddus C, Myers G. Cell detection with star-convex polygons. MICCAI 2018 - 21st International Conference, Granada, Spain, September 16–20, 2018, Proceedings, Part II. SpringerLink; 2018. https://doi.org/10.1007/978-3-030-00934-2_30.
22. Rakaee M, Kilvaer T, Dalen S, et al. Evaluation of tumor-infiltrating lymphocytes using routine H&E slides predicts patient survival in resected non-small cell lung cancer. Hum Pathol 2018;79. https://doi.org/10.1016/j.humpath.2018.05.017.
23. Gataa I, Mezquita L, Rossoni C, et al. Tumour-infiltrating lymphocyte density is associated with favourable outcome in patients with advanced non-small cell lung cancer treated with immunotherapy. Eur J Cancer (Oxford, England: 1990) 2021:145. https://doi.org/10.1016/j.ejca.2020.10.017.
24. Dieci M, Radosevic-Robin N, Fineberg S, et al. Update on tumor-infiltrating lymphocytes (TILs) in breast cancer, including recommendations to assess TILs in residual disease after neoadjuvant therapy and in carcinoma in situ: a report of the International Immuno-Oncology Biomarker Working Group on Breast Cancer. Semin Cancer Biol 2018;52(Pt 2). https://doi.org/10.1016/j.semcancer.2017.10.003.
25. Salgado R, Denkert C, Demaria S, et al. The evaluation of tumor-infiltrating lymphocytes (TILs) in breast cancer: recommendations by an International TILs Working Group 2014. Ann Oncol Off J Eur Soc Med Oncol 2015;26(2). https://doi.org/10.1093/annonc/mdu450.
26. Kos Z, Roblin E, Kim R, et al. Pitfalls in assessing stromal tumor infiltrating lymphocytes (sTILs) in breast cancer. NPJ Breast Cancer 2020:6. https://doi.org/10.1038/s41523-020-0156-0.
27. Wein L, Savas P, Luen S, Virassamy B, Salgado R, Loi S. Clinical validity and utility of tumor-infiltrating lymphocytes in routine clinical practice for breast cancer patients: current and future directions. Front Oncol 2017:7. https://doi.org/10.3389/fonc.2017.00156.
28. Homeyer A, Geißler C, Schwen L, et al. Recommendations on compiling test datasets for evaluating artificial intelligence solutions in pathology. Mod Pathol Off J US Can Acad Pathol, Inc 2022;35(12). https://doi.org/10.1038/s41379-022-01147-y.
29. Altini N, Marvulli M, Zito F, et al. The role of unpaired image-to-image translation for stain color normalization in colorectal cancer histology classification. Comput Methods Prog Biomed 2023. https://doi.org/10.1016/j.cmpb.2023.107511.
30. Janowczyk A, Zuo R, Gilmore H, Feldman M, Madabhushi A. HistoQC: an open-source quality control tool for digital pathology slides. JCO Clin Cancer Inform 2019:3. https://doi.org/10.1200/CCI.18.00157.
31. Jahn S, Plass M, Moinfar F. Digital pathology: advantages, limitations and emerging perspectives. J Clin Med 2020;9(11). https://doi.org/10.3390/jcm9113697.
32. Smits A, Kummer J, de Bruin P, et al. The estimation of tumor cell percentage for molecular testing by pathologists is not accurate. Mod Pathol Off J US Can Acad Pathol, Inc 2014;27(2). https://doi.org/10.1038/modpathol.2013.134.